Size and surface effects on the magnetic properties of NiO nanoparticles

Mariana P. Proenca[a,b], Célia T. Sousa[a], André M. Pereira[a], Pedro B. Tavares[c], João Ventura[a], Manuel Vazquez[b], João P. Araujo*[a]

[a] IFIMUP and IN – Institute of Nanoscience and Nanotechnology and Dep. Física e Astronomia, Univ. Porto, Rua do Campo Alegre 687, 4169-007 Porto, Portugal

[b] Instituto de Ciencias Materiales de Madrid, CSIC, 28049 Madrid, Spain

[c] Dep. Química e CQ-VR, Univ. Trás-os-Montes e Alto Douro, 5001-801 Vila Real, Portugal

Corresponding author: Prof. João P. Araújo, jearaujo@fc.up.pt

Table of contents entry

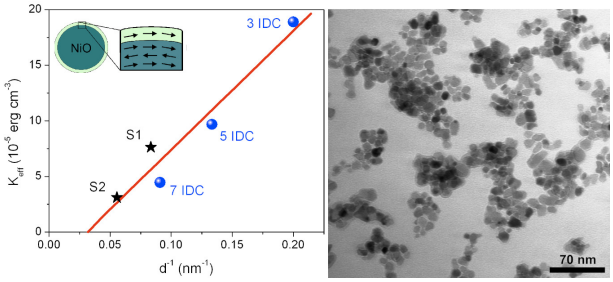

We demonstrate the existence of uncompensated spins with ferromagnetic correlations at the surface of the NiO nanoparticles coupled to their antiferromagnetic core and we estimate the surface anisotropy constant for small nanoparticle diameters using a recent model.

Abstract

NiO nanoparticles (NPs) were prepared by a sol-gel process using the citrate route. The sol-gel parameters were tuned to obtain samples with different average particle sizes, ranging from 12 to 70 nm. Magnetic characterization revealed an increase in the blocking temperature with the diameter of the NPs and an increase in the effective magnetic anisotropy (K_{eff}) with decreasing particle size. The magnetic moment per particle was calculated for all samples using the susceptibility value at T=300 K. The number of uncompensated spins per NP was found to be proportional to $n_S^{1/3}$ ($n_S \equiv$ total number of spins), indicating that they are randomly distributed on the NP surface. For small diameters (<30 nm) the surface anisotropy constant was estimated, using, for NiO NPs, a recent model describing the evolution of K_{eff} with particle size. Hysteretic loops performed at low temperatures after field cooling displayed loop shifts (~6.5 kOe in the field axis and ~0.18 emu g^{-1} vertically), coercive field enhancement (H_C~4.8 kOe) and training effects for the smaller NPs. The sample with NPs of larger diameters presented magnetic properties close to those of bulk NiO.

1. Introduction

Nickel oxide (NiO) is a promising material, extensively used in catalysis, battery cathodes, gas sensors and electrochromic films.[1-5] Furthermore, bulk NiO is an antiferromagnetic (AFM) material with a Néel temperature of 523 K and can thus be used in a variety of magnetic applications, particularly as a pinning layer in spin valves and magnetic tunnel junctions.[6] Nanostructured AFM oxides have therefore recently gained increased attention.[7,8] When the dimensions of AFM oxides are decreased into the nanoscale, they start to exhibit a variety of new physical phenomena, such as weak ferromagnetism (FM) arising from the surface and finite size effects or a net magnetic moment coming from uncompensated spins. This surface effect was first studied by L. Néel in 1961, when he inferred that small particles of an AFM material should exhibit superparamagnetism (SPM)

and weak FM, and attributed the permanent magnetic moment to uncompensated spins in the two sublattices.[9] However, the 2-sublattice model was not able to fully explain the observed large magnetic moments, enhanced coercivity and hysteretic loop shifts found in AFM nanoparticles (NPs) at low temperatures. These results were then explained by a multi-sublattice spin configuration model,[10] that besides being able to account for the high net magnetic moment experimentally observed, also allowed the occurrence of a variety of magnetization reversal paths when cycling the applied magnetic field (H), thus explaining coercivity enhancement and loop shift.[11] These two latter phenomena are a consequence of the so-called exchange bias effect that appears when a FM or a spin-glass (SG) like surface shell is exchange coupled to an AFM core.[12,13] There have been recent discussions on whether NiO NPs should exhibit SPM or SG behaviours, since their magnetization cannot be well described by the modified Langevin function.[14] Detailed studies on the magnetic and time dependent properties of NiO NPs concluded that they indeed show SG behaviour, originating from the freezing of the NPs surface spins.[15-17] In addition, Néel also found that the number of uncompensated spins (q) depends on the crystal structure and particle morphology, and considered three different models.[18,19] If the uncompensated spins are randomly distributed in the particle, one expects $q \propto n_S^{1/2}$ (where n_S is the total number of spins). If they are arranged parallel to each other in an odd number of layers stacked in a cube, then $q \propto n_S^{2/3}$. Finally, if the core of the particles has no defects, and the uncompensated moments are randomly distributed at the surface, then one has $q \propto n_S^{1/3}$. The nature of the anomalous effects observed in the NiO NPs is still under discussion but it was already confirmed that the magnetic behaviour largely depends on their method of preparation and on the presence/absence of coatings on their surface.[16,17,20]

In this work we synthesised NiO NPs with controlled diameters using a sol-gel procedure.[21,22] Crystalline NiO NPs were obtained, as confirmed by both transmission electron microscopy (TEM) and X-ray diffraction (XRD). The smaller nanoparticles (12-18 nm in size) were found to be spherical in shape and could be well dispersed, while the larger

ones (40-100 nm) had irregular shapes and tended to agglomerate. Magnetization measurements of the obtained NiO NPs both as a function of temperature *M(T)* (from 5 to 370 K) and applied magnetic field *M(H)* (at 300 and 6 K), after zero-field (ZFC) and field-cooling (FC), were performed. The smaller NPs showed a temperature below which the ZFC and FC magnetization split, due to the freezing of uncompensated spins. A peak in the ZFC *M(T)* curve was also verified, associated with the blocking temperature (T_B) of the NPs. Such temperature was found to increase with NP diameter. From the magnetic susceptibility and particle size measurements, we found $q \propto n_S^{1/3}$, indicating that the uncompensated spins are randomly distributed at the surface of the NP. We also extracted the effective magnetic anisotropy (K_{eff}) of the NPs and confirmed the presence of strong contributions from the surface.[23,24] Finally, enhanced coercivity, hysteretic loop shifts and training effects,[25-29] associated with the exchange bias effect, were found for the smaller NPs at low temperatures, denoting the presence of a FM shell / AFM core exchange coupling.

2. Experimental

NiO NPs were synthesized by a sol-gel method using $Ni(NO_3)_2.6H_2O$ as precursor and citric acid as ligand.[21] A first solution was prepared by dissolving measurable $Ni(NO_3)_2.6H_2O$ in deionised water and a second solution by dissolving citric acid in deionised water. The latter was then added dropwise to the first at room temperature and under magnetic stirring. The molar ratio of citric acid to nickel nitrate (c:n) was 1:4 (samples S1 and S3) and 1:1 (sample S2). The pH value was adjusted only in sample S3 by adding NH_4OH. The final solution was stirred and heated at 343 K overnight for the aging of the gel. Finally, the solution was dried at 373 K for 24 h and calcined at 673 K (sample S1) and 773 K (samples S2 and S3) for 4 h. Table 1 summarizes the preparation parameters used for each sample.

The morphologies and distributions of the NiO NPs were observed by TEM (LEO 906E), using an accelerating voltage of 100 kV. Structural analysis was performed by XRD (PW 3040/60 X'Pert Pro Röntgen diffractometer) using Cu Kα radiation (λ=0.15418 nm) and the

Bragg–Brentano θ/2θ geometry. The system includes an ultra-fast X'Celerator detector PW3015/20 and a secondary monochromator. Magnetic measurements were preformed on a superconducting quantum interference device (SQUID) magnetometer from Quantum Design, both as a function of temperature [*M(T)*; from 5 to 370 K] and applied magnetic field [*M(H)*; at 300 and 6 K], after ZFC and FC at 10 kOe.

3. Results and discussion

3.1 Structural characterization

The size and shape of the produced nanoparticles were obtained using TEM. Spherical and dispersed NiO NPs were observed for samples S1 and S2 [Figs. 1(a) and (b)]. The average diameter of such spherical nanoparticles (D_{TEM}) was estimated using *ImageJ*[30] to obtain the histogram of the size distribution. This histogram was then fitted to a log-normal distribution [lower inset of Fig. 1(a)], allowing us to obtain for S1 and S2, D_{TEM}~13.6 and 19.5 nm, respectively (Table 1). In sample S3 the particles were agglomerated and exhibited a more irregular shape with larger dimensions, making it harder to determine their sizes, although an average value of 70 ± 30 nm could be estimated. Upper insets of Fig. 1 correspond to electron diffraction (SAED) patterns of the NiO NPs, where rings can be observed, confirming the presence of polycrystalline NiO.

Crystallographic measurements performed using XRD confirmed the formation of face-centred cubic (fcc) NiO with space group *Fm3m*, and lattice parameter $a_0 \approx 0.4188$ nm, in close agreement with the reported value for bulk NiO (~0.4178 nm).[31] Fig. 2(a) shows the diffraction patterns obtained for the different synthesized samples, presenting the reflections characteristic of NiO and evidencing the quality of the samples. The average crystallite size of the particles (D_{XRD}) was calculated using the Williamson-Hall relationship:[32]

$$\beta_{total} = \beta_{size} + \beta_{strain} = \frac{k\lambda}{D_{XRD}\cos\theta} + 4\eta\tan\theta, \quad (1)$$

where β_{total} is the full width at half-maximum of the XRD peak, k the Scherrer constant for spherical NPs (~0.94), λ the incident X-ray wavelength, θ the diffraction angle and η the

microstrain parameter. Fig. 2(b) shows a plot of $\frac{\beta_{total}\cos\theta}{k\lambda}$ vs. $\frac{4\sin\theta}{k\lambda}$ for all samples, allowing the estimation of D_{XRD} and η (Table 1). The values obtained for D_{XRD} are in good accordance with the ones measured by TEM. Internal strain is also present for all samples, however it can be considered negligible [η (%) < 0.2 %] and therefore does not play a significant role in the main physical properties of these nanomaterials.[33]

3.2 Magnetic characterization

Temperature dependent magnetization *M(T)* measurements were performed for all samples under zero-field- and field-cooling conditions, from 370 to 5 K. Fig. 3(a), (b) and (c) show the *M(T)* curves obtained for samples S1, S2 and S3, respectively.

For samples S1 and S2 one finds a peak, in the ZFC magnetization curves, together with a bifurcation between FC and ZFC data below a certain temperature. This behaviour is typically present in an assembly of ferromagnetic-like nanoparticles exhibiting superparamagnetism above a certain temperature. The peak in the ZFC curve is usually associated with the mean blocking temperature (T_B), that decreases with the size of the NPs [T_B~270 K for 18 nm (sample S2), ~200 K for 13 nm (S1) and ~50 K for 7 nm (according to ref. 34)]. The joining of the ZFC and FC curves at the so-called irreversible temperature (T_{IRR}), above which all spins are unblocked, usually marks the highest blocking temperature of the ensemble, *i.e.* the largest nanoparticle present. We also found a decrease of T_{IRR} with decreasing NP size [T_{IRR}~330 K for 18 nm (sample S2), ~250 K for 13 nm (S1) and ~200 K for 7 nm (according to ref. 34)].

For sample S3 (larger average NP diameter), no bifurcation was found in the FC and ZFC magnetizations in the measured temperature range [Fig. 3(c)]. In fact, a paramagnetic (PM) behaviour is found in the whole temperature range, as typically observed in bulk NiO samples.[13] This PM behaviour can be attributed to the incomplete compensation of the AFM sublattices at the surface.[35] Notice that a similar PM behaviour can also be seen in the low temperature regime of the *M(T)* curves of samples S1 and S2 [Figs. 3(a) and (b)], as

revealed by the sharp *M*-increase with decreasing *T*. This low temperature behaviour can be associated with the presence of uncorrelated PM spins at the surface that undergo a magnetic transition to a collective spin state at low temperatures, plus suggesting that the large magnetization values measured are related with broken exchange bonds and reduced coordination at the surface.

In Fig. 4 one shows the susceptibility obtained directly by $\chi = \frac{M}{H}$ [since the *M(T)* measurements were performed under a low applied magnetic field (H<50 Oe)], showing that the NPs with smaller diameters present higher susceptibilities. This can be further inferred from the inset of Fig. 4, where the magnetic susceptibility is seen to decrease with the inverse of the NPs average size, with a slope of 2.28x10^{-4} emu g^{-1} Oe^{-1} nm^{-1}. This result agrees well with that of Richardson *et al.*,[36] where a slope of 2.38x10^{-4} emu g^{-1} Oe^{-1} nm^{-1} was obtained.

To extract information on the uncompensated surface contribution, we can consider that (as a first approximation) the susceptibility is given by:[18]

$$\chi_{total} = \frac{n\mu_0}{3k_B T} < \mu_{NP}^2 > + \chi_{bulk}, \quad (2)$$

where *n* is the number of nanoparticles per gram, μ_0 the permeability of free space, k_B the Boltzmann constant, μ_{NP} the magnetic moment per particle and χ_{bulk} the susceptibility of bulk NiO (~9.7x10^{-6} emu g^{-1} Oe^{-1} at 295 K)[37]. Considering the 295 K susceptibility for the 3 samples and using eqn (2), we estimate a magnetic moment per particle of ~390 μ_B, 550 μ_B and 1470 μ_B for S1, S2 and S3, respectively (where μ_B is the Bohr magneton). Now taking into account μ=2 μ_B per Ni^{2+} ions, we calculate the number of uncompensated Ni^{2+} ions per NP, resulting in ~195, 275 and 735 for S1, S2 and S3 samples, respectively. The total number of Ni^{2+} ions per particle was also estimated considering fcc NiO with a lattice parameter $a_0 \approx 0.4188$ nm and spherical NPs of diameter D_{XRD}, allowing us to plot $\ln q$ vs. $\ln n_S$ and the corresponding fit with slope 1/3 [inset of Fig. 3(c)]. Considering the Néel

relation on the nature of the uncompensated spins,[18,19] the good fit obtained indicates that the uncompensated spins occur randomly on the surface of the NP ($q \propto n_S^{1/3}$).

Therefore, we can conclude that the bifurcation in the ZFC and FC curves for S1 and S2 samples also comes from surface effects, mainly due to the presence of uncompensated surface spins (USS).

The magnetic properties of SPM NPs are very sensitive to interparticle interactions.[38] However, in the case of our AFM NPs, the magnetic moments were found to be too small for dipolar interactions to significantly affect the obtained results.[39] In fact, the energy of the dipolar interactions can be estimated using:[40]

$$U_{\text{int}} = \frac{\mu_0 \mu_{NP}^2}{4\pi d_p^3} \cos 45^\circ, \tag{3}$$

where d_p is the distance between the particles. Using the magnetic moment calculated from eqn (2) and considering $d_p \sim D_{XRD}$, we estimate $U_{int} \sim (0.4\text{-}3.3) \times 10^{-6}$ eV. This corresponds to a negligible critical temperature between 0.004 K (S1) and 0.04 K (S3). The dipolar interactions in our samples can thus be ignored, making them unique for the study of exchange coupling within magnetic particles.

Considering isolated SPM particles, we can define the blocking temperature as:[41]

$$T_B = \frac{K_{eff} V_{NP}}{k_B \ln(\tau_m / \tau_0)}, \tag{4}$$

where K_{eff} is the effective magnetic anisotropy constant, V_{NP} the volume of the NP, τ_m the characteristic measurement time (~10 s for SQUID measurements) and τ_0 the characteristic SPM relaxation time (~10^{-10} s). Using the values of T_B for S1 and S2 we estimated $K_{eff} \sim 6.00 \times 10^5$ and 3.05×10^5 erg cm^{-3}, respectively. These show the expected tendency to increase as the particle size decreases.[23,42] Since the surface-to-volume ratio is higher for smaller NPs, surface effects start to govern the magnetic properties when their size is reduced. Considering that the uncompensated spins are located at the surface of the NP, occupying a shell of thickness t_{Shell} and volume V_{Shell} (inset scheme of Fig. 5), we can assume:

$$K_{eff} \propto \frac{K_S}{t_{Shell}}\left(\frac{V_{Shell}}{V_{NP}}\right), \quad (5)$$

below a certain NP diameter (d_c), where K_S is the surface anisotropy constant.[12] One thus has $K_{eff} \propto \frac{K_S}{d}$ in the limit where the NP diameter (d) is very small. Fig. 5 shows the evolution of K_{eff} with d^{-1}, where data from ref. 43 was added for better comparison. Such simplified model shows the importance of the surface anisotropy contribution, giving a surface anisotropy constant of K_S~1.1 erg cm^{-2} and a critical diameter of d_c~32 nm, above which bulk behaviour regains importance. However, the value of K_S was found to be higher than the one predicted for NiO.[12] For the same reason, Tobia *et al.* proposed a new model for AFM Cr_2O_3 NPs that takes into consideration other important changes that the particles undergo when their size is reduced:[24]

$$K_{eff} \propto \frac{K_S}{t_{Shell}}\left(\frac{V_{Shell}}{V_{NP}}\right)^2. \quad (6)$$

They found a good fitting for t_{Shell} of the order of the lattice parameter. Considering then $t_{Shell} \approx 0.4188$ nm, we obtain K_S~(0.40±0.04) erg cm^{-2}, in close agreement with the values reported elsewhere for NiO thin films.[12] These results further support the fact that the uncompensated spins are indeed located at the surface of the NPs, and therefore largely contribute to the effective magnetic anisotropy constant.

Hysteretic loops *M(H)* were also measured for the smaller NPs (S1 and S2) at 300 K exhibiting a typical SPM behaviour (Fig. 6). The magnetization curves, above the blocking temperature, are usually fitted using a Langevin function,[38] allowing the estimation of the magnetic moment per particle. For FM and ferrimagnetic NPs, this model gives a good approximation. However, in AFM NPs, where the magnetic moments are relatively small, the anisotropy energy becomes more evident, and the *M(H)* curves present significant deviations from the Langevin function.[23,44] In weakly uncompensated AFM particles, the uncompensated magnetic moments must be considered as fluctuating essentially along the AFM axis. However, in the Langevin model, the uncompensated moments are assumed to rotate freely.

Therefore, the parameters obtained using the Langevin function for AFM NPs can be incorrect. The other method here used [eqn (2)] is thus more appropriate for the estimation of the magnetic moment per NP.

Magnetization curves *M(H)* were also measured at 6 K after ZFC and FC (Fig. 6). The non-saturation behaviour of the curves, also seen at 300 K, is associated with the AFM core behaviour of the NPs. However, an extra contribution coming from the USS can also be detected at low temperatures. The coupling between the AFM core and the USS is evidenced by the remarkable enhancement of the coercive field (H_C) and loop shift observed at 6 K after FC with an applied field of 10 kOe. The loop shift is characterized by an exchange bias field H_{EX}, here defined as $H_{EX} = -\left(H_{C1} + H_{C2}\right)/2$, where H_{C1} and H_{C2} are the left and right coercive fields, respectively, and by a vertical shift, defined as $M_{EB} = \left(M_{\max} + M_{\min}\right)/2$, where M_{max} and M_{min} are the maximum and minimum magnetization values (obtained at high field), respectively.[34] For sample S1, we obtained H_C^{FC}~4.8 kOe, H_C^{ZFC}~2.5 kOe, H_{EX}~6.5 kOe and M_{EB}~0.18 emu g^{-1}, while for sample S2 smaller values of H_C, H_{EX} and M_{EB} were found (H_C^{FC}~1.0 kOe, H_C^{ZFC}~0.2 kOe, H_{EX}~2.9 kOe and M_{EB}~0.10 emu g^{-1}). These results demonstrate the increase importance of the USS when the NPs size is decreased. In fact, when increasing the surface-to-volume ratio, one expects that the effect of the USS becomes more evident, as experimentally observed. Since T_B of both samples is below room temperature, lowering the temperature from 370 to 5 K with an applied field blocks the USS in one direction. The resulting unidirectional anisotropy (below T_B) between the FM coupled USS and the AFM core provides a pinning force against spin reversal, leading to the shift of the hysteresis loop. The increase of H_C with the decreasing size of the NPs is in accordance with the splitting found in the ZFC and FC *M(T)* curves, that reflects the remanence of the spin system, and shows the same tendency with the NPs size.

Finally, we also observed the so-called training effect for both samples S1 and S2 (Fig. 6). Measuring two consecutive magnetic hysteretic cycles after FC, one observes a drop of H_C^{FC} and H_{EX} from 4550 and 5950 Oe (1st cycle) to 3620 and 4880 Oe (2nd cycle),

respectively, in sample S1 and from 990 and 2880 Oe (1st cycle) to 795 and 2665 Oe (2nd cycle), in S2. Such training effect is often observed in AFM/FM exchange systems and explained as the rearrangement of the (metastable) spin structure of the AFM layer with each reversal of the FM layer magnetization. This leads to a partial loss of its net magnetization and, thus, to a reduction of the exchange bias. Our results then suggest irreversible spin rearrangements with field cycling, likely occurring in the disordered spin surface.

4. Conclusions

In this paper we have discussed the magnetic properties of NiO nanoparticles with different sizes. Temperature dependent magnetization measurements showed a bifurcation in the ZFC and FC curves for smaller NPs, corresponding to a superparamagnetic behaviour. The blocking temperature was found to increase with the diameter of the NPs, so that, for the samples with larger diameters, no T_B was observed below 370 K. The magnetic moment per particle was estimated for all samples using the susceptibility value at T=300 K. The number of uncompensated spins per NP was found to be proportional to the cubic root of the total number of spins, suggesting that the uncompensated spins occur randomly on the NP surface. The effective anisotropy extracted from the T_B values showed a tendency to increase as the particle size decreases (from K_{eff} ~$3x10^5$ to $6x10^5$ erg cm^{-3} when the NP size goes from 18 to 13 nm). The surface anisotropy constant (K_S~0.40 erg cm^{-2}) was estimated for NiO NPs. Magnetic hysteretic loops measured at 6 K after FC illustrated an enhancement in the coercive field, a loop shift and training effect (higher and more evident for the smaller NPs). Our results demonstrate the existence of uncompensated spins with FM correlations at the surface of the NP coupled to the AFM core, therefore exhibiting an exchange bias behaviour similar to the one observed in FM/AFM bilayers.

Acknowledgements

M. P. Proença and C. T. Sousa are thankful to Fundação para a Ciência e a Tecnologia (FCT) for doctoral grants SFRH/BD/43440/2008 and SFRH/BD/38290/2007, respectively. A.

M. Pereira is thankful to FCT for postdoctoral grant SFRH/BPD/63150/2009. J. Ventura acknowledges financial support through FSE/POPH. J. P. Araújo also thanks the Fundação Gulbenkian for its financial support within the 'Programa Gulbenkian de Estímulo à Investigação Científica'. The authors acknowledge funding from FCT through the Associated Laboratory – IN and project ref. PTDC/QUI-QUI/105304/2008.

References

1. R. M. Gabr, A. N. El-Naimi, M. G. Al-Thani, *Thermochim. Acta*, 1992, **197**, 307.
2. M. Yoshio, Y. Todorov, K. Yamato, H. Noguchi, J. Itoh, M. Okada and T. Mouri, *J. Power Sources*, 1998, **74**, 46.
3. S. Ikeda, T. Takata, M. Komoda, M. Hara, J. N. Kondo, K. Domen, A. Tanaka, H. Hosono and H. Kawazoe, *Phys. Chem. Chem. Phys.*, 1999, **1**, 4485.
4. H. Steinebach, S. Kannan, L. Rieth, F. Solzbacher, *Sensor. Actuat. B-Chem.*, 2010, **151**, 162.
5. A. C. Sonavane, A. I. Inamdar, P. S. Shinde, H. P. Deshmukh, R. S. Patil and P. S. Patil, *J. Alloy. Compd.*, 2010, **489**, 667.
6. A. E. Berkowitz and K. Takano, *J. Magn. Magn. Mater.*, 1999, **200**, 552.
7. V. Skumryev, S. Stoyanov, Y. Zhang, G. Hadjipanayis, D. Givord and J. Nogués, *Nature*, 2003, **423**, 850.
8. J. Nogues, J. Sort, V. Langlais, V. Skumryev, S. Surinach, J. S. Munoz and M. D. Baro, *Phys. Rep.*, 2005, **422**, 65.
9. L. Neel, in *Low Temperature Physics*, ed. C. Dewitt, B. Dreyfus and P. D. de Gennes, Gordon and Beach, New York, 1962, p. 413.
10. R. H. Kodama, S. A. Makhlouf and A. E. Berkowitz, *Phys. Rev. Lett.*, 1997, **79**, 1393.
11. R. H. Kodama, *J. Magn. Magn. Mater.*, 1999, **200**, 359.
12. J. Nogues, I. K. Schuller, *J. Magn. Magn. Mater.*, 1999, **192**, 203.
13. M. Jagodič, Z. Jagličić, A. Jelen, J. B. Lee, Y.-M. Kim, H. J. Kim and J. Dolinšek, *J. Phys.: Condens. Matter*, 2009, **21**, 215302.
14. S. A. Makhlouf, F. T. Parker, F. E. Spada and A. E. Berkowitz, *J. Appl. Phys.*, 1997, **81**, 5561.
15. S. D. Tiwari and K. P. Rajeev, *Phys. Rev. B*, 2005, **72**, 104433.

16. E. Winkler, R. D. Zysler, M. Vasquez Mansilla, D. Fiorani, D. Rinaldi, M. Vasilakaki and K. N. Trohidou, *Nanotechnology*, 2008, **19**, 185702.
17. V. Bisht and K. P. Rajeev, *J. Phys.: Condens. Matter*, 2010, **22**, 016003.
18. C. R. H. Bahl, M. F. Hansen, T. Pedersen, S. Saadi, K. H. Nielsen, B. Lebech and S. Mørup, *J. Phys.: Condens. Matter.*, 2006, **18**, 4161.
19. L. Neel, *Compt. Rend.*, 1961, **252**, 4075.
20. M. Ghosh, K. Biswas, A. Sundaresan and C. N. R. Rao, *J. Mater. Chem.*, 2006, **16**, 106.
21. Y. Wu, Y. He, T. Wu, T. Chen, W. Weng and H. Wan, *Mater. Lett.*, 2007, **61**, 3174.
22. Q. Yang, J. Sha, X. Ma and D. Yang, *Mater. Lett.*, 2005, **59**, 1967.
23. C. Gilles, P. Bonville, K. K. W. Wong and S. Mann, *Eur. Phys. J. B*, 2000, **17**, 417.
24. D. Tobia, E. De Biasi, M. Granada, H. E. Troiani, G. Zampieri, E. Winkler and R. D. Zysler, *J. Appl. Phys.*, 2010, **108**, 104303.
25. S. Brems, D. Buntinx, K. Temst, C. Van Haesendonck, F. Radu, and H. Zabel, *Phys. Rev. Lett.*, 2005, **95**, 157202.
26. F. Radu, M. Etzkorn, R. Siebrecht, T. Schmitte, K. Westerholt, and H. Zabel, *Phys. Rev. B*, 2003, **67**, 134409.
27. J. Ventura, J. P. Araujo, J. B. Sousa, A. Veloso, P. P. Freitas, *Phys. Rev. B*, 2008, **77**, 184404.
28. N. J. O. Silva, A. Millán, F. Palacio, M. Martins, T. Trindade, I. Puente-Orench and J. Campo, *Phys. Rev. B*, 2010, **82**, 094433.
29. M. P. Fernández-García, P. Gorria, M. Sevilla, A. B. Fuertes, R. Boada, J. Chaboy, G. Aquilantid and J. A. Blanco, *Phys. Chem. Chem. Phys.*, 2011, **13**, 927.
30. W. S. Rasband, ImageJ, U. S. National Institutes of Health, Bethesda, Maryland, USA, http://rsb.info.nih.gov/ij/, 1997-2009
31. S. Sasaki, K. Fujino, and Y. Takeuchi, *P. Jpn. Acad. B-Phys.*, 1979, **55**, 43.
32. H. Bi, S. Li, Y. Zhang and Y. Du, *J. Magn. Magn. Mater.*, 2004, **277**, 363.
33. P. Kameli, H. Salamati and A. Aezami, *J. Appl. Phys.*, 2006, **100**, 053914.
34. S. K. Sharma, J. M. Vargas, E. De Biasi, F. Béron, M. Knobel, K. R. Pirota, C. T. Meneses, S. Kumar, C. G. Lee, P. G. Pagliuso and C. Rettori, *Nanotechnology*, 2010, **21**, 035602.
35. E. Winkler, R. D. Zysler, M. Vasquez Mansilla and D. Fiorani, *Phys. Rev. B*, 2005, **72**, 132409.

36. J. T. Richardson, D. I. Yiagas, B. Turk, K. Forster and M. V. Twigg, *J. Appl. Phys*., 1991, **70**, 6977.
37. W. J. Schuele and V. D. Deetscreek, *J. Appl. Phys*., 1962, **33**, 1136.
38. S. Mørup, D. E. Madsen, C. Frandsen, C. R. H. Bahl and M. F. Hansen, *J. Phys.: Condens. Matter*., 2007, **19**, 213202.
39. M. F. Hansen, C. B. Koch and S. Mørup, *Phys. Rev. B*, 2000, **62**, 1124.
40. A. M. Pereira, C. Pereira, A. S. Silva, D. S. Schmool, C. Freire, J.-M. Greneche and J. P. Araujo, submitted.
41. G. C. Papaefthymiou, E. Devlin, A. Simopoulos, D. K. Yi, S. N. Riduam, S. S. Lee and J. Y. Ying, *Phys. Rev. B*, 2009, **80**, 024406.
42. J. M. D. Coey, in *Magnetism and Magnetic Materials*, Cambridge University Press, New York, 2010.
43. N. M. Carneiro, W. C. Nunes, R. P. Borges, M. Godinho, L. E. Fernandez-Outon, W. A. A. Macedo and I. O. Mazali, *J. Phys. Chem. C*, 2010, **114**, 18773.
44. N. J. O. Silva, V. S. Amaral and L. D. Carlos, *Phys. Rev. B*, 2005, **71**, 184408.

Tables

Sample	pH	Molar ratio (c:n)	Calcination Process		Particle size by XRD (nm)	Particle size by TEM (nm)	Strain by XRD (10^4)
			Temperature (K)	Heating Rate (K/min)			
S1	2.0	1:4	673	1	12.8 ± 0.6	13.6 ± 1.0	9.25
S2	2.0	1:1	773	1	18.4 ± 0.3	19.5 ± 1.0	7.62
S3	6.8	1:4	773	10	60.3 ± 2.2	70 ± 30	11.8

Table 1. Preparation conditions used for each sample during sol-gel process and respective particle size and lattice strain estimated by XRD and TEM.

Figures

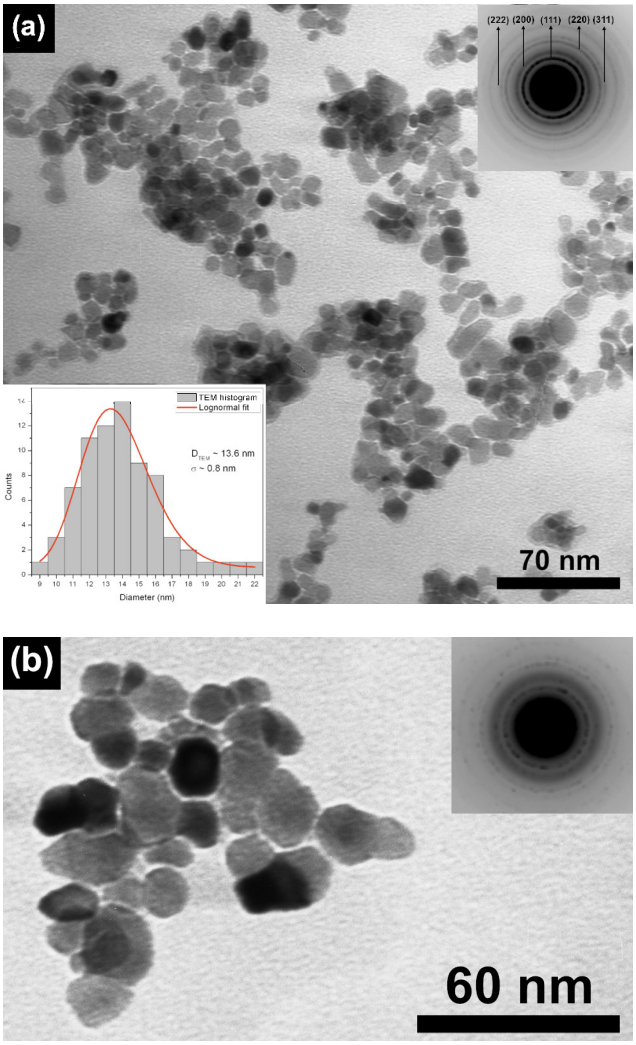

Fig. 1. TEM images of sample S1 (a) and S2 (b). Lower inset on (a) shows the respective histogram of the particles' size distribution and a log-normal fit. Upper insets on both images show the corresponding SAED where the usual rings of polycrystalline NiO can be identified.

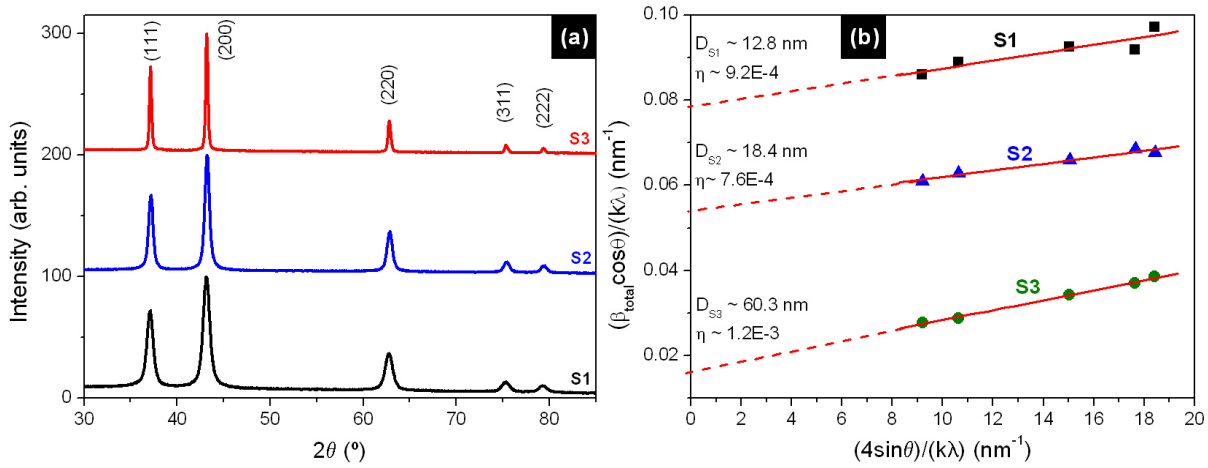

Fig. 2. (a) XRD pattern of the NiO NPs synthesized and (b) linear fit using the Williamson-Hall correlation (the different slopes represent different mean strains and the line interception gives the inverse particle size).

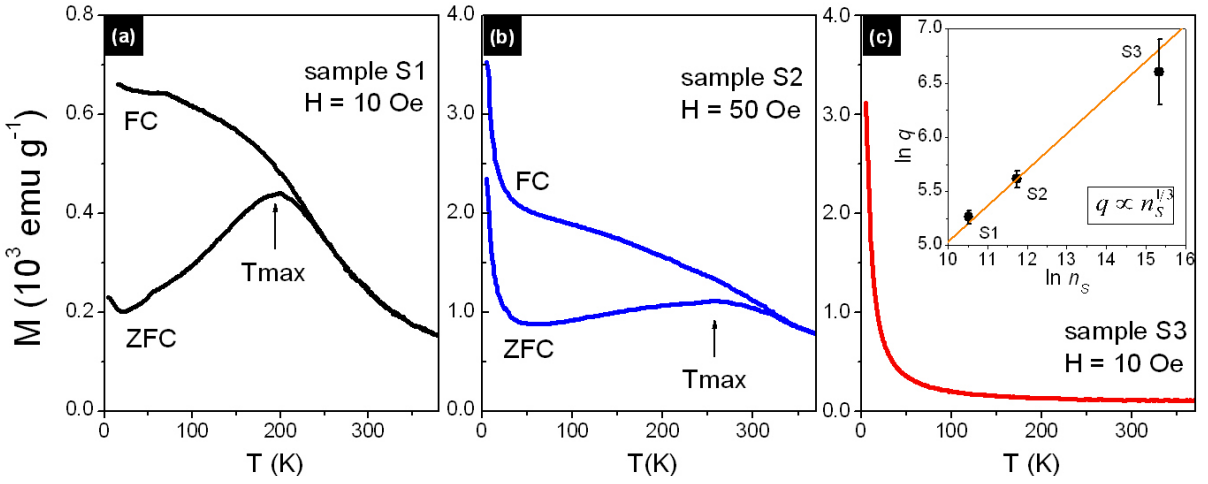

Fig. 3. ZFC and FC magnetization measurements of samples S1 (a), S2 (b) and S3 (c). Inset shows the relation between the number of uncompensated spins q and the total number of spins n_S in a small particle, showing that $q \propto n_S^{1/3}$.

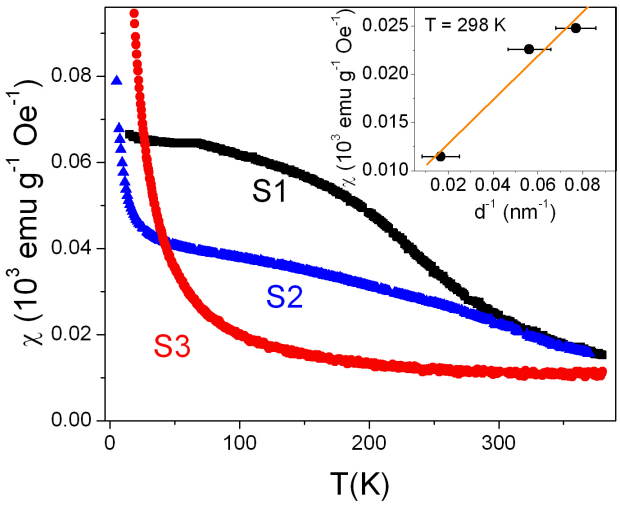

Fig. 4. Variation of magnetic susceptibility with temperature for all samples. Inset shows the linear variation of magnetic susceptibility with the inverse of the NPs' size at 298 K.

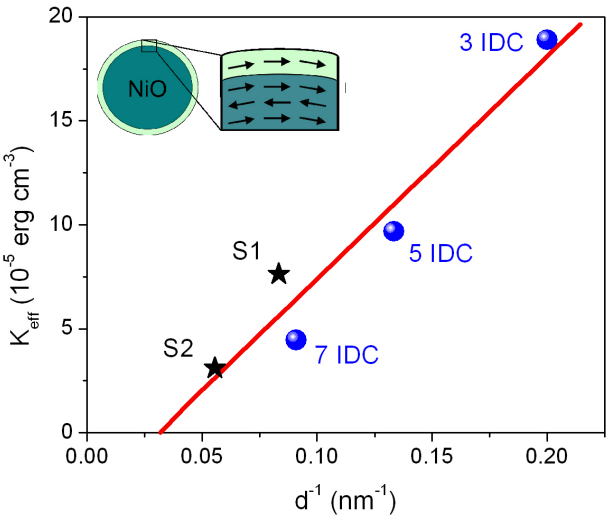

Fig. 5. Variation of the effective magnetic anisotropy with the inverse diameter of small NiO NPs. Samples 3, 5 and 7 IDC are taken from ref. 43. Inset scheme illustrates the NiO NP formed by a shell of uncompensated spins with FM correlations and an AFM core.

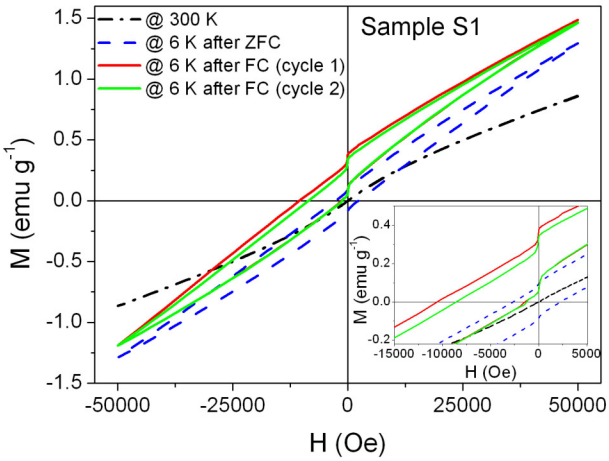

Fig. 6. Magnetic hysteresis loop of sample S1 at 300 K (black dash-dotted line) and at 6 K after ZFC (blue dashed line) and after FC with an applied field of 10 kOe (lines: red – 1st cycle and green – 2nd cycle). Inset shows a detail of the hysteresis loop around zero field, evidencing the exchange bias and training effect found after FC.